IOSR Journal of Applied Geology and Geophysics (IOSR-JAGG)
e-ISSN: 2321–0990, p-ISSN: 2321–0982.Volume 4, Issue 6 Ver. II (Nov-Dec. 2016), PP 21-35
www.iosrjournals.org

Geochemistry of the Tholeiite and Alkaline Dykes of Nongryngkoh-Padu-Jarain Area, Meghalaya, North East India: Evidence for Kerguelen plume-involvement in an Extensional Regime

M.A. Khonglah[1], Sougrakpam Sujata[1], Imlishila Imchen[2] and R. Baskaran[3]
[1]*Geological Survey of India, Petrology Laboratory, North Eastern Region, Shillong.*
[2]*Geological Survey of India, State-Unit Meghalaya, North Eastern Region, Shillong.*
[3]*Geological Survey of India, State Unit-Kerela, Southern Region, Thiruvananthapuram.*

Abstract: *Episodic network of dykelets/dykes/sills intrude the Precambrians of Padu-Nongryngkoh-Jarain area, East Meghalaya Plateau, North East India; close to a weak intersection zone of Raibah and Umngot faults in an extensional phase caused by upwelling of the Kerguelen Plume. Olivine and diopside macrocrysts/microcrysts and xenocrysts with calcite or, analcite ocelli dispersed in a tholeiitic or, alkali basaltic or, alkaline base implies a rapid and violent ascent to the surface. The dykes are picritic, tholeiitic, alkaline to occasionally calc-alkaline. The ultramafic and some of the alkaline dykes are abundant in compatible elements, along with high Mg# suggesting a primitive source while mildly enriched LILE (e.g., Sr, K, Rb, Ba, Th), HFSE (e.g., Nb & Zr) and LREE (e.g., La, Ce, Sm) with depleted HFSE (e.g., Ti & Y) and HREE infers crustal contribution of the more evolved tholeiitic and some alkaline samples. The attribute of these alkaline-OIB type dykes infers a mantle derived magma ascending to the surface with some melting, assimilation, storage and homogenization (MASH). Modest to abundant rare-earth elements ($\sum REE$ = ~ 80 to 332 ppm, La_N = 50 to 225) increases from the picritic to tholeiitic to calc-alkaline samples; a manifestation of assimilation and fractional crystallization (AFC). The alkaline dykes with higher REE contents than the tholeiitic counterparts are derived from an enriched mantle. Moderately high REE fractionation with high $(Gd/Yb)_{CN}$ ratios indicates garnet fractionation that could be linked to a plume-related mantle sources that melted at depths of the garnet [$(Gd/Yb)_{CN} > 2$] facies; supported by considerable HREE depletion compared to LREE $(La/Yb)_{CN}$. These REE characteristics corroborate to the garnet peridotite sourced basalt flows of Mawsynram-Shella basalts of East Khasi Hills section and Rajmahal-II basalts related to the Kerguelen Plume activity.*

Keywords: *Early Cretaceous Sylhet Trap, tholeiites, alkali basalt, nephelinite.*

I. Introduction

The Meghalaya-Assam Plateau exposes rock types ranging from Archaean, Proterozoic to Tertiary period. The Precambrian Gneissic Complex (GC) comprises dismembered caught up patches of meta-pelite (sillimanite-corundum rock, khondalite), calc-granulites and two pyroxene granulites and charnockite (Gogoi, 1975; Khonglah, et al, 2008, Khonglah, et al, 2010) occurring within undifferentiated gneisses (older grey biotite metapelitic gneiss, tonalitic-granodioritic gneiss & younger pinkish K-rich granite gneiss) unconformably overlain by metasediments of the Shillong Group (SG). The 'Khasi Metabasic Intrusives' of gabbroic composition at places associated with meta-hornblendite-tonalite-trondhjemite are confined to the Shillong Group (Khonglah, et al, 2012). Several Mid to Late Proterozoic porphyritic granitoid plutons in association with anorthositic-rock/norite/noritic-gabbro – quartz-mangerite - charnockite (Khonglah, et al, 2010) and other mafic differentiates (Sarkar, et al, 2007) and Early Cretaceous ultramafic–alkaline–carbonatite complexes intrude both the GC and SG (Nandy, 2001). The southern part of the massif is covered by the Sylhet trap volcanics and Tertiary sedimentary sequences (Talukdar, & Murthy1971; Nandy, 2001) (Fig-1). Locally, two distinct alkali basalt flows occur in the Umiew and Dwara gorge section between the more dominant tholeiitic basalt flows (Talukdar, 1967).

The communication aims at documenting the preliminary petrography and geochemical characters of the hitherto unknown network of ultrabasic-basic-alkaline dykes/dykelets and sills (Fig-3) of Nongryngkoh-Padu-Jarain area (*henceforth refer to as NPJA*), which are hypabyssal representatives of the Early Cretaceous Sylhet Trap basalt flows (Fig-2). These picro-tholeiitic basalt (PB)[Fig-4] some with alkaline affinity (APB); high Mg-tholeiitic basalt (TB), tephrite basanite (TBN), alkali olivine basalt (AB) [Fig-3], nephelinite (NP), tholeiitic basalt (TB), basalt (B), dolerite (D), trachy-basalts (TRB) and basaltic andesite (BA) dykelets/dykes/sills are intrusive into the Precambrians. Locally the oldest rock types in NPJA comprises banded metasedimentary carbonate - calc-silicate - silicate supracrustals rocks (*henceforth refer to as* ***BCS***)

included in older grey granodioritic mylonitic gneiss *(refer to as OG)* with both possibly forming the basement rocks for the Proterozoic SG metasediments. Younger sheared, foliated augen and pinkish syntectonic granites *(refer to as YG)* emplace the BCS and OG. This composited granitoid complex occupies the area south of Umngot River. The green schist facies quartzite, micaceous quartzite, thin quartz-mica-schist intercalations of SG and Khasi Meta-Basics *(refer to KMB)* situates north of the Umngot River (Fig. 2, present work). However caught-up-patches of SG quartzite, KMB within YG prevail south of the river, e.g. WNW of Padu (Fig-2). Locally the carbonate of BCS are remobilized and injected into the YG and KMB in the form of small dykelets, veins and *lit-per-lit* injections. Late phase syn to post tectonic pegmatites intrudes the BCS, OG, SG and YG followed by the Cretaceous dykes mentioned above. The thick bedded Tertiary sandstones of Shella Formation unconformably blankets the Proterozoic and Cretaceous rocks (Fig-2). The BCS and OG maintain a NW-SE and ENE-WSW foliation trends in the Umngot Gorge and Umsiang Riverbeds respectively, while bedding and mylonitic foliation of SG vary from ENE-WSW to NE-SW with steep northerly dips. The contact between the SG and YG is intrusive and subsequently thrusted along ENE-WSW, evidenced by presence of recumbent folds in SG near to the contact and development of an ENE-WSW trending shear zone along the contact. The Tertiary sandstones display a sub-horizontal to horizontal bedding attitude (Fig-2).

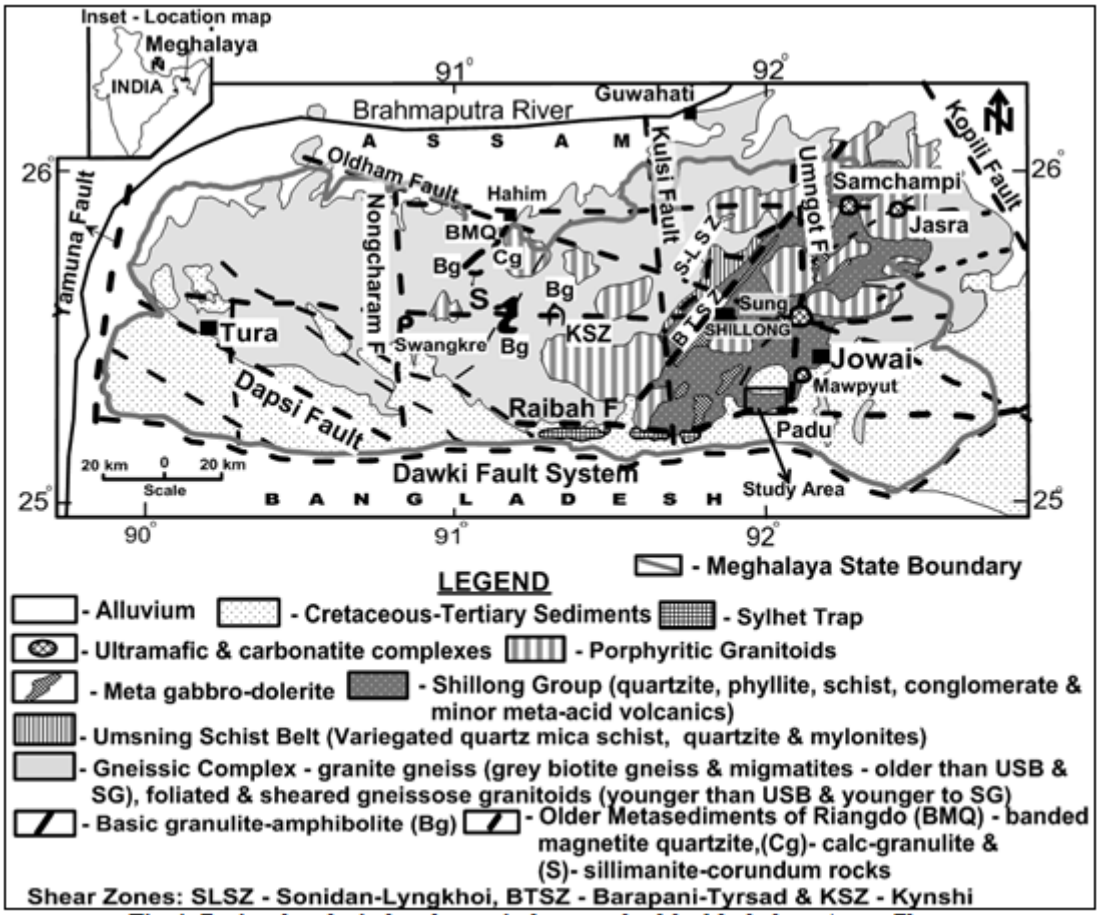

Fig- 1. Regional geological and tectonic framework of the Meghalaya-Assam Plateau
(modified after Mazumdar, 1976, Nandy, 2001, Srivastava, et al, 2004 & Khonglah, et al, 2008)

The network of NPJA dykes, occasionally sills (Fig-3) intrude the Precambrians along ENE-WSW; NNE-SSW, NW-SE and rarely along N-S trends close to an intersection zone of two major linear structures involving the eastern extension of the E-W striking Raibah fault (Talukdar & Murthy, 1971; Nandy, 2001) meeting the N-S trending Umngot Fault [Srivastava, et al, 2004] (Fig-1 & 2). The thicknesses of the dykes vary from 5 cm to > 1 m never exceeding 1.5 m. Chilled margins and xenoliths of granitoids are associated with the thicker dykes. Megascopically the porphyritic basalt dykes are melanocratic and cumulitic to porphyritic in nature with phenocrysts of up to ~50 to 60% by volume in picro-tholeiitic basalt; ~ 30 to 40% in tholeiitic basalt TB and widely varying from ~ 20 to 50% in tephrite basanite, alkali olivine basalt and trachy-basalts. Euhedral to subhedral mafic phenocrysts of ~ 0.5 - 1cm length scatter in a microcrystalline to glassy basalt groundmass dotted with pyrite and rare galena specks. Megascopically the nephelinite, dolerites and non-porphyritic basalt dykes are melanocratic and medium to fine grained sparsely spotted with pyroxene, plagioclase or rarely olivine

phenocrysts in case of the latter two. The basaltic andesite dykelet at Jarain intruding augen granite is leucocratic and fine grained while at Umgnot Riverbed NNW of Mawlong it is mesocratic (present work).

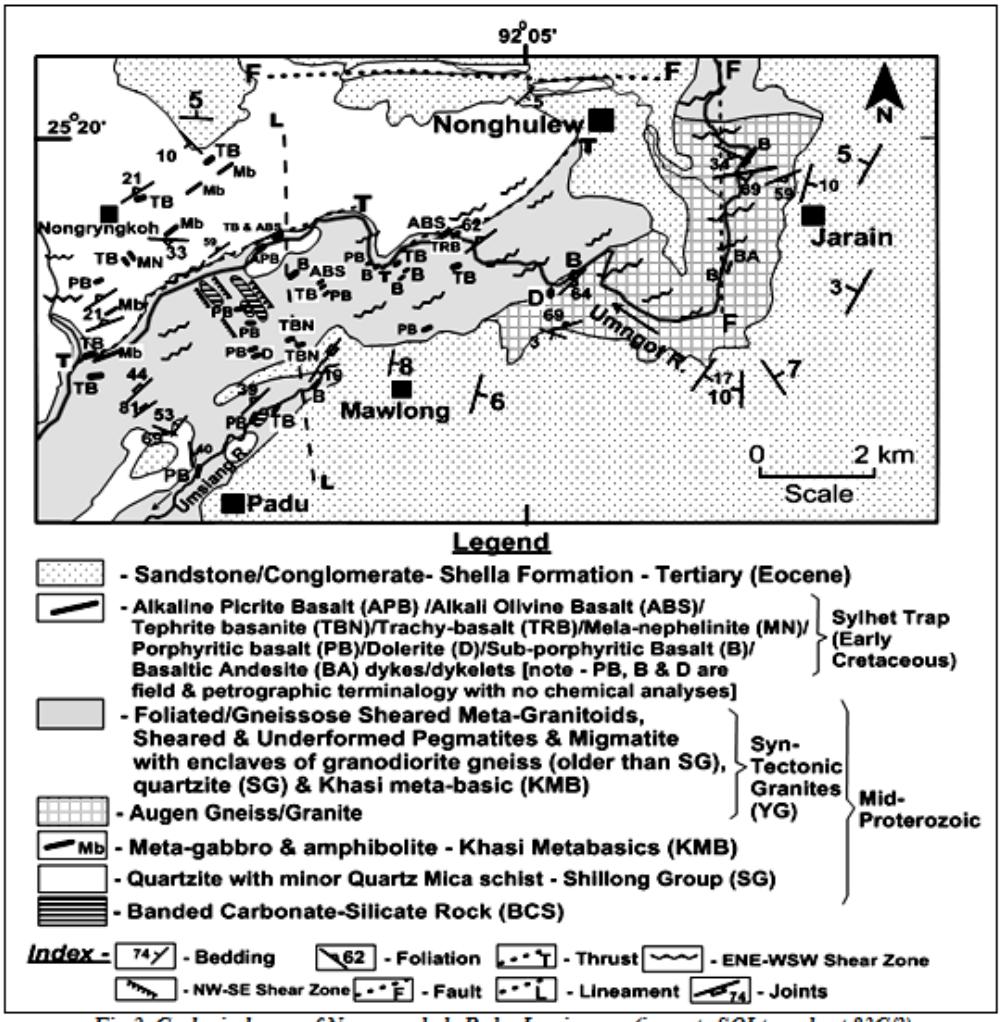

Fig-2. Geological map of Nongryngkoh-Padu-Jarain area (in parts SOI toposheet 83C/3), Jaintia & East Khasi Hills Districts, Meghalaya.

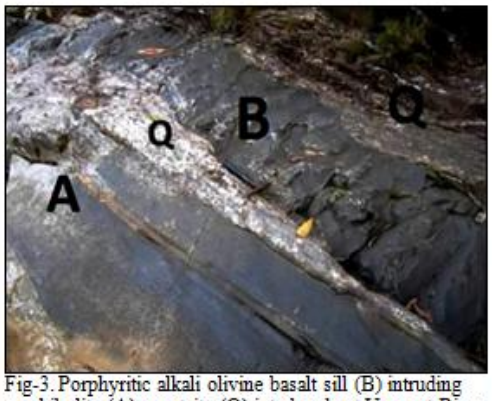

Fig-3. Porphyritic alkali olivine basalt sill (B) intruding amphibolite (A)-quartzite (Q) interbands at Umngot River, NNW of Mawlong

Fig-4. Olivine and Cpx macrocrysts set in a basalt groundmass of alkaline-picro-basalt of Umsiang River.

Petrography & Mineral Phase Identification: Thin section studies were carried out with the aid of Orthoplan & Leica binocular microscope while EPM Analysis was taken up for mineral species identification at EPMA Laboratory, Central Headquarters, GSI, Kolkata, with a CAMEMCA Sx100 instrument at accelerating voltage of 15 KV, current of 12 *nA* and beam size of 1 micron where all natural standards were maintained except for

Mn and Ti, which is synthetic. The porphyritic basaltic dykes constitute variable proportions of euhedral to subhedral macrocrysts (>1000 µm) of olivine (chrysolite *Fo ~78-83 for picro-tholeiitic basalt ; Fo ~86 for tholeiitic basalt*), [Fig-5 & 6], diopside (*En~ 30-41, Wo ~ 45-50, Fs~ 5-22 & occasionally En~48, Wo~49 & Fs~3)* with presence of augite (*En~39-49, Wo~51-60 & Fs~10-17*) in picro-basalt. Oscillatory and sector zoning are pronounced in the Cpx xenocrysts (Fig-7), macrocrysts and microcrysts that may poikilitically enclose olivine (Fig-7). In picro-basalt and tholeiitic basalt the microcrystalline groundmass, constitute Cpx (diopside of similar composition to macrocrysts), opaques (magnetite and ilmenite), plagioclase, ± analcite, biotite, calcite, titanite, serpentinised talcose-chloritic-, clayey materials (mostly of montmorillonite-smectite composition with occasional kaolinite & illite) and mafic glass. Only minor plagioclase (labradorite - *An~50 to 57*) [Fig-5] associates with picro-tholeiitic basalt that increases in TB and the non-porphyritic basalt dykes. In tephrite basanite, alkali olivine basalt and trachy-basalts, glassy mafics (mainly pyroxene), analcite, K-feldspar and clayey material makes up the groundmass. In both basic and alkaline dykes an oxide phase (*i.e.,* magnetite) exists as subhedral to euhedral or, acicular to skeletal grains with rare exsolution texture. Amoeboid, elliptical, circular to irregular ocelli of calcite and ocelli of similar composition to the groundmass commonly occur in the groundmass. Analcite ocelli encasing calcite grains a (Fig-8) associate with the alkaline dykes e.g. tephrite basanite and nephelinite. In nephelinite diopside (*En~48, W~50, Fs~2*) phenocrysts are set in a medium grained groundmass of spongy nepheline, microcrystic diopside and occasional wollastonite (*En~32-38, Wo~50-55, Fs~10-12*), opaques and minor to accessory biotite, apatite, secondary altered brownish ferruginised material, spinel and hydro-garnet (Fig-9). Globular calcite ocelli some with excellent pseudo-uniaxial figure (Fig-9) are partially embayed by elongated diopside and spongy nepheline grains (Fig-9). Hydro-garnet (grossular ~ 83 and spessartite ~ 16) occur as secondary anhedral altered products around Cpx and associates with the dusty ferruginous patches formed due to post magmatic metasomatic/alteration reactions. In the non-porphyritic basaltic and dolerite dykes sparse euhedral macrocrysts/xenocrysts and microcrysts of plagioclase > clino-pyroxene spreads in a fine to medium grained, ophitic to sub-ophitic basic base. The basaltic andesite samples petrographically constitute widely scattered globular vesicles/ocelli filled up by polygonal aggregates of secondary calcite distributed in a groundmass of feldspar glass shards and microlites, intensely spotted with fine mafic minerals and opaques (magnetite). Common accessories in the samples are mainly apatite, zircon and sphene. In one sample, a pyrite ocellus is included in a bigger calcite ocellus (Fig-10) implicating complex immiscible coexistence of andesitic basalt magma, carbonate melt and a sulphide liquid phase.

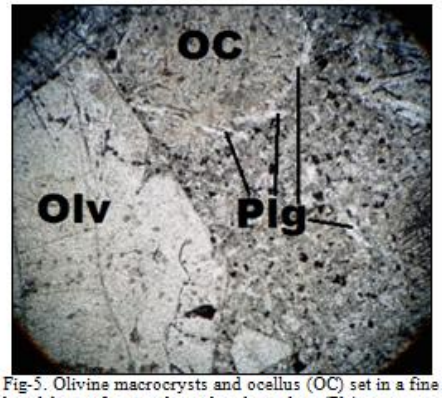

Fig-5. Olivine macrocrysts and ocellus (OC) set in a fine basalt base of augite, diopside, plagioclase (Plg), opaques, chlorite and glass of picro-basalt. (6.3x10 magnification)

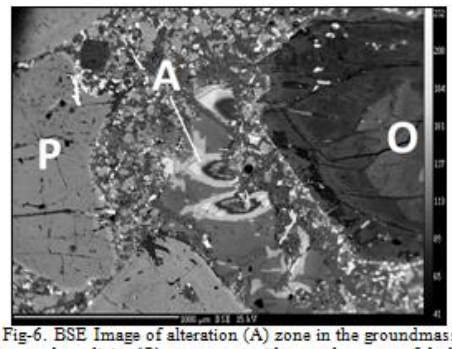

Fig-6. BSE Image of alteration (A) zone in the groundmass around an olivine (O) macrocryst with complex zone of dark talcose and lighter carbonate bands. P - Diopside corroded macrocrysts; groundmass comprises microcrysts of diopside, opaques (ilmenite, Ti-magnetite and rare chromite) & minor plagioclase.

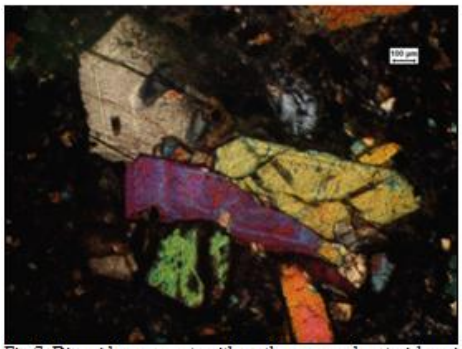
Fig-7. Diopside xenocrysts with partly preserved sectorial zoning set in a Cpx, analcite and opaque rich dark groundmass in alkali basalt.

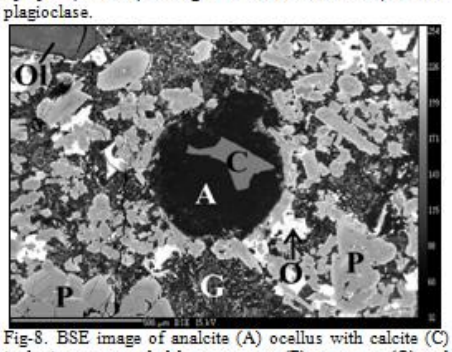

Fig-8. BSE image of analcite (A) ocellus with calcite (C) inclusion surrounded by pyroxene (P), opaques (O) and occasional olivine (Ol) microcrysts, fine fibrous groundmass (G) of diopside, analcite, K-feldspar, clay minerals, chlorite and dark glassy groundmass (towards the right side of photograph) in porphyritic tholeiitic basalt of Nongryngkoh.

II. Geochemistry

Methodology:

The Major oxides and trace-element (Ba, Ga, Sc, V, Th, Pb, Ni, Co, Rb, Sr, Y, Zr, Nb, Cr, Cu and Zn) bulk analysis of the representative samples were analyzed by a fully automated X-ray fluorescence (XRF), PANalytical model MagiX-2424 using end window X-ray tube at the Chemical Division, Geological Survey of India, North Eastern Region, Shillong. The remaining samples were analyzed by Atomic Absorbtion Spectrometry (AAS) method in the Chemical Division; Geological Survey of India, North Eastern Region, Shillong. The REE were analyzed by Inductively Coupled Plasma Emission Mass Spectrometer (ICP-MS) in the Chemical Laboratory; Geological Survey of India, Central Headquarter, Kolkata. The details of techniques, procedure, precision and accuracy of these analyses are described in SOP (http://www.portal.gsi.gov.in/, GSI, 2010). Field relations, major-minor oxides, trace and RE element behaviours suggest the basaltic dykes/dykelets of the area can be sub-divided into three batches.

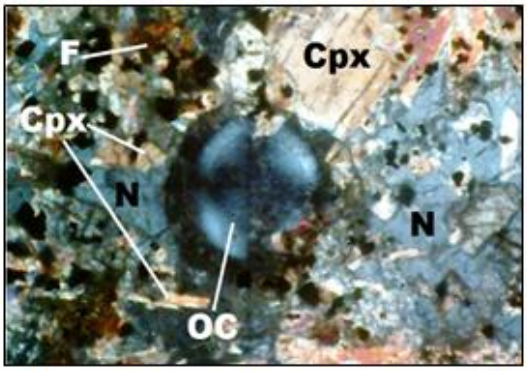

Fig-9. Calcite ocellus with pseudo-uniaxial cross partially embayed by Cpx & nepheline (N) in nephelinite. F – secondary ferruginous material with hydro-garnet formed around Cpx and opaques mainly Ti-magnetite. (magnification 10 x 10).

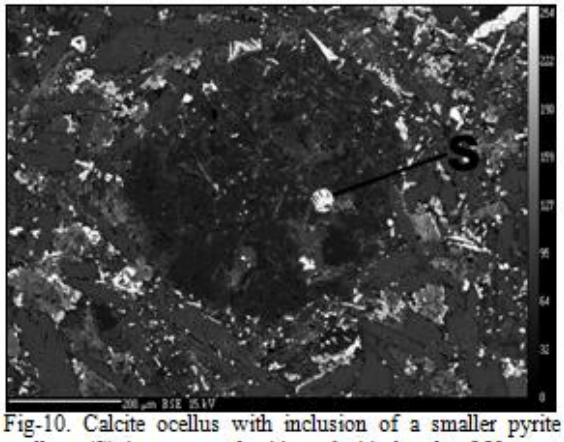

Fig-10. Calcite ocellus with inclusion of a smaller pyrite ocellus (S) in non-porphyritic andesitic basalt of Umngot River Section.

Major oxide geochemistry: Collectively, the basic and alkaline dykes are silica-undersaturated. In the TAS binary plot of Le Bas, et al, (1986), the porphyritic samples are alkaline to sub-alkaline (tholeiitic), while the non-porphyritic dykes are mostly tholeiitic, as illustrated by the Irvine & Baragar, (1971) division line (Fig-11). They classify as tholeiitic and alkali basalt with the occasional spill-over into the picro-basalt, tephrite basanite and trachybasalt fields. Two of the non porphyritic samples feature in the basaltic andesite domain (Fig-11). Most samples are sodic with Na_2O/K_2O ratio of >1 (Table – I & II); primarily controlled by the groundmass analcite in the basaltic samples and nepheline in nephelinite. However, three samples (one sample of picro-basalt, tephrite basanite and basaltic andesite) are potassic with Na_2O/K_2O ratio of < 1, contributed by groundmass K-feldspar and clayey minerals. High MgO wt%, Mg#, Ni, Cr, and strong normative olivine and pyroxene of picro-basalt, high Mg-tholeiite and few alkali olivine basalt samples are in part largely attributed by the cumulitic or, phenocrystic (macrocrystic) and xenocrystic phases. The picritic and tholeiitic samples are typically hypersthene normative (Table - I & II). Overall, the porphyritic alkali olivine basalt samples register lower MgO wt%, CaO wt%, Ni and Cr contents but higher Al_2O_3 wt% compared to picro-basalt and high Mg-tholeiitic basalts but have similar contents to the more evolved tholeiites, advocating probable different magma source (Winter, 2001, p-275-276). One calc-alkaline basaltic andesite sample of Jarain is potassic (Na_2O/K_2O = 0.42). The samples has wide ranging Fe_2O_3(T) and TiO_2 wt %, that slightly increase from picro-basalt to tholeiitic basalt to tephrite basanite to alkali olivine basalt to basaltic andesite. The nephelinite sample with highest normative nepheline (Ne=20.95); has moderate diopside, low olivine and low leucite in the norm (Table-II) with low Cr and Ni contents too. Well-defined coherent negative trend display by SiO_2 vs. Mg# and positive plot of CaO vs. Mg# (Fig-12) of the samples suggest normal magmatic differentiation trends.

Trace and REE geochemistry: Chondrite normalised REE diagrams (after Nakamura, 1974) display three different profiles of similar mild fractionation trends invoking three pulsated dyke activities in NPJA; for the purpose of convenience these are categorise as B-1, B-2 & B3; with B-1. B-1 register a weak Sm positive anomaly (Fig-13) while B-2 records a smoother pattern (Fig-13.1) without any Eu anomaly implying suppression of plagioclase; while a prominent Eu negative anomaly indicate plagioclase fractionation for B-3 (Fig-13.2). A single sample of high Mg-tholeiite dyke [AJ-6A (m)] exhibits lower LREE and higher HREE distribution with a flat profile when compared to other B-1 samples suggesting its mantle origin that is also supported by its high MgO, Mg#, Ni and Cr contents. The REE profiles of all samples are comparable to those

of Mawsynram-Balat and Rajmahal-II basalts (Fig-13.3). Enriched LREE with respect to depleted HREE typifies normal fractionation, comparable to alkali basalts and alkaline rocks (Sun, & McDonough, 1989; Culler & Graf, 1984; Kontak, et al, 2001). The minimum and maximum LREE enrichment $(La/Yb)_{CN}$ ranges in the three groups are 5.06 in picro-basalt and 15.15 in alkali olivine basalt of B-1; 11.73 in picro-basalt and 14.83 in alkali olivine basalt of B-2 and 11.25 in a picro-basalt and 15.64 in basaltic andesite of B-3 respectively, with nephelinite of B-2 showing a maximum ratio of $(La/Yb)_{CN}$ =16.8 consistent with alkaline basalts (Culler & Graf, 1984; Sun & McDonough, 1989). The rock chondrite normalised trace elemental spider diagram (Sun, 1980) for NPJA dykes compare well to the average typical alkali OIB (Fig-14) but are more enriched in Rb, Ba and Th as expected of these continental alkaline basalts (Fig-14) suggesting some crustal contributions (De Paolo, 1981). The samples are mildly enriched in LILE (e.g., Sr, K), HFSE (e.g., Nb & Zr) and LREE (e.g., La, Ce & Sm); slightly impoverished in HFSE (e.g., Ti & Y) and strongly depleted in HREE. The the Nb/Y vs. Zr/TiO_2 binary plot suggest (Winchester & Floyd, 1977) an alkali basalt source [Fig-14.1] for the samples.

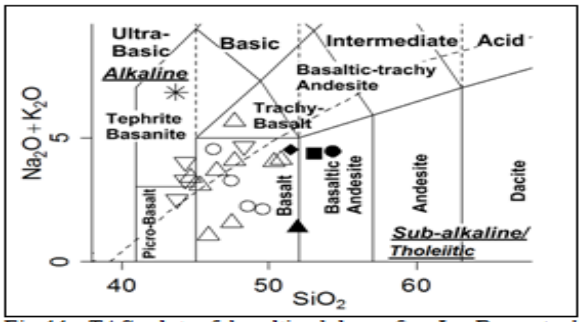

Fig-11. TAS plot of basaltic dykes after Le Bas, *et al*, (1986). The alkaline-sub-alkaline divide is from Irvine and Baragar (1971). ***Symbols: B1*** - [open triangle - porphyritic basaltic dykes, dark triangle – high Mg-tholeiitic basalt intruding BCS]; ***B2*** [open circle - porphyritic basaltic dykes, dark circle - non-porphyritic to sparsely porphyritic basalt & asterix - nephelinite]; ***B3*** [inverted triangle- porphyritic basaltic dykes, black diamond – non-porphyritic basalt & black square - andesitic basalt].

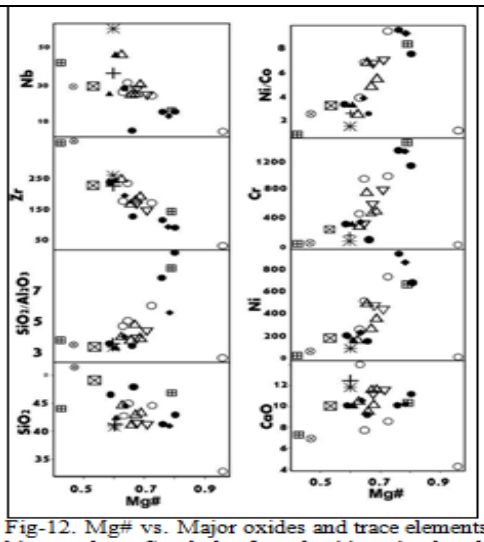

Fig-12. Mg# vs. Major oxides and trace elements binary plots. Symbols: [porphyritic- picrobasalt (cross-square), tholeiite basalt (black dots), alkali olivine basalt (open triangle) & tephrite basanite (plus) of B-1], [porphyritic- tholeiite basalt (open circles), alkali olivine basalt (black triangle) and nephelinite (asterix) of B-2] & porphyritic-picro-basalt (black dots), alkali tephrite basanite (open inverted triangle), non-porphyritic alkali basalt (diagonal cross-square) & andesitic basalt (cross square) of B-3.

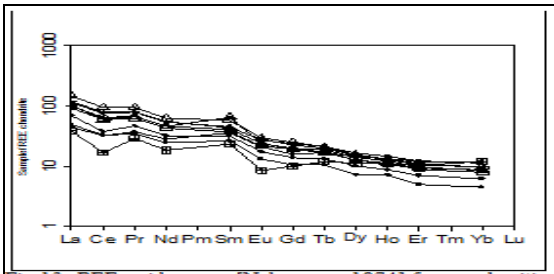

Fig-13: REE spidergram [Nakamura, 1974] for porphyritic-picro-basalt (cross-square), tholeiite basalt (black dots) and alkali basaltic dykes (open triangle) of B-1.

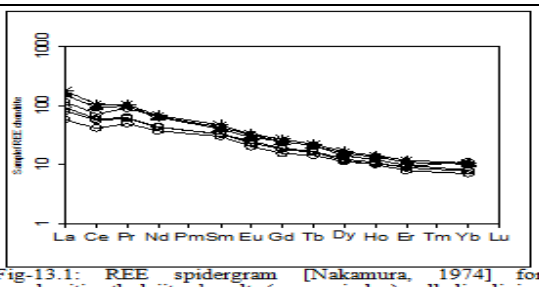

Fig-13.1: REE spidergram [Nakamura, 1974] for porphyritic tholeiite basalt (open circles), alkali olivine basalt (black triangle) and nephelinite (asterix) of B-2.

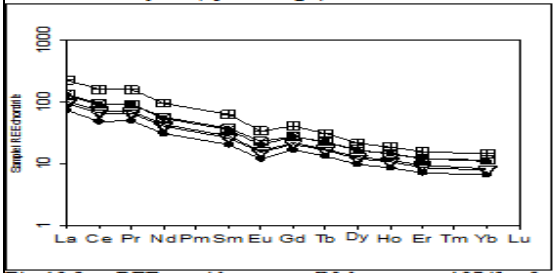

Fig-13.2: REE spidergram [Nakamura, 1974] for porphyritic- picro-basalt (black dots), alkali tephrite basanite (open inverted triangle), non-porphyritic alkali basalt (diagonal cross-square) & andesitic basalt (cross square) of B-3.

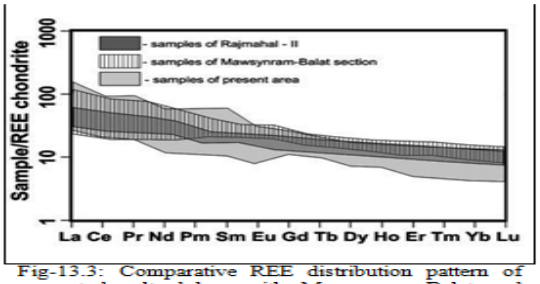

Fig-13.3: Comparative REE distribution pattern of present basalt dykes with Mawsynram-Balat and Rajmahal - II basalts

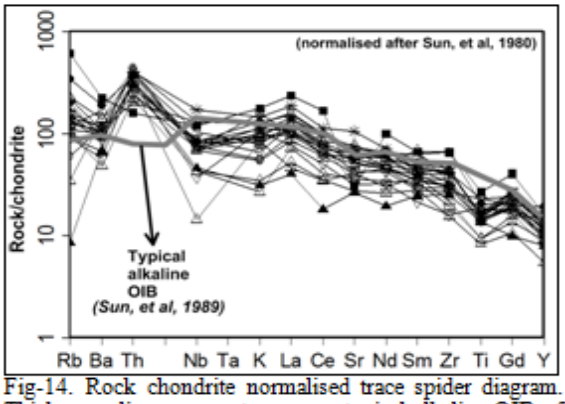

Fig-14. Rock chondrite normalised trace spider diagram. Thick grey line represents average typical alkaline OIB of Sun & McDonough, 1989. Symbols as in Fig-11.

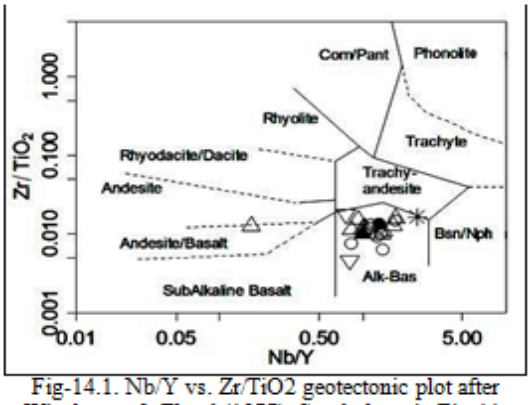

Fig-14.1. Nb/Y vs. Zr/TiO2 geotectonic plot after Winchester & Floyd (1977). Symbols as in Fig-11.

Tectonic setting and Petrogenesis: Intersection of two major linear structures (present work) involving the E-W striking Raibah Fault (Nandy, 2001) and the N-S, Umngot Fault (Srivastava, et al, 2004) (Fig-1 & 2), west of Jarain, rendered the Nongryngkoh-Padu-Jarain (NPJA) study area susceptible to episodic picritic, tholeiitic to alkaline basaltic dyke activities during the Early Cretaceous Sylhet Trap volcanism that took place in an extensional phase caused by upwelling of the Kerguelen Plume (Nambiar, 2007). The first pulse probably commenced with intrusion of high Mg-tholeiitic to tholeiitic and trachy-basalt followed by alkaline basalt dykes; the second episode initiated with tholeiitic basalt, basalt andesite, alkaline basalt and nephelinite while the third cycle comprise alkaline-picro-basalt followed by tholeiitic basalt, basaltic andesite and alkaline basalt. These cycles of tholeiite and alkaline activities are consistent with generation of OIBs, more specifically, alkaline island and continental OIBs (Winter, 2001, p-275-276). The alkaline basalt constituting mainly tephrite basanite, alkali olivine basalt and nephelinite are correctable with the middle Sylhet Trap alkaline alkali olivine basalt flow (Talukdar, 1971). The episodic and simultaneous activities are evidenced by parallel orientation of porphyritic alkali olivine basalt alongside non-porphyritic tholeiitic basalt in the Umngot River, NNW of Mawlong; *or*, a basaltic andesite dykelet paralleling an older tholeiitic basalt dyke, west of Jarain of the same river (Fig-2). In each case the dykes are separated by a gap of < 1m. Abundant reaction/resorbtion/corroded textures in the xenocrysts/macrocrysts testify to an interaction of early formed olivine (Fig-6) and diopside (Fig-7) with later melts, in both picritic-tholeiitic and alkaline dykes. Coexistence of analcite ocelli with encased calcite grains and occasional analcite phenocrysts in tephrite basanite, alkali olivine basalt and to a less extent in porphyritic tholeiite basalt (Fig-8) advocate immiscibility involving picritic-tholeiitic-basalt; alkaline and minor carbonate melts at some stage during evolution of the dykes; which again provided clues for different sources for the alkaline and tholeiite dykes. Similarly, calcite ocelli in nephelinite strongly implied immiscibility of alkaline and minor carbonate melts (Fig-9). The nephelinite dykes with abundant anhedral to spongy nepheline with poikilitically enclosed pyroxenes and other opaques indicate late phase alkaline activity during the second cycle activity of B2 that is familiar to the late phase nepheline syenite activity documented from Mawpyut ultramafic complex (Moitra, et al, 2011). Similar periodic alkaline activities are documented from the three shields of Hawaii Mauna Kea, Hualalai and Kohala) where caldera collapse in the waning stage activity had produced more episodic, violent and alkaline lavas (Winter, 2001). These lavas are more diverse, with shallow fractionation producing rocks ranging from alkaline rocks to trachyte that are prevalent in NPJA. This stage may be followed by a long period of dormancy (0.5 to 2.5 Ma) a late, post-erosional stage takes place that is characterised by silica undersaturated highly alkaline magmas including alkali basalts, basanites, nephelinites, and nepheline melilites of which with exception of nepheline melilites all are found NPJA. The sequential effusion of tholeiite later making way to an alkaline trend is in agreement to volcanic islands on mature oceanic crust setting and plume related models (Winter, 2001 p. 275-276, Fig-15.2). The transition from tholeiites to alkaline magmas is created by a high degree of partial melting of a shallow source followed by less extensive partial melting of a deeper source as activity waned which is in tune with experimental data (Winter, 2001; pg. 275- 276 & references therein). Talukdar (1971), described alkali basalt layers sandwiched between the lower and upper tholeiitic basalt flows that once again is in accordance to those described from Hawaii Island (Winter, 2001). Groundmass, ocelli and occasional phenocrystic analcite to a less extent albite are the main mineral phase contributing to the sodic nature of samples along to the moderate to high normative nepheline in tephrite basanite and alkali olivine basalt; while groundmass K-feldspar is responsible for the elevated K_2O contents of some of the potassic samples. Abundance of analcite ocelli and occasional crystalline phase suggest possible magmatic origin transitional between primary magmatic (P type) and hydrothermal (H type) analcimes (Demeny, et al, 1997). Melluso, et al, (2010) indicated parageneses formed by batches of primitive magmas with

a distinct magmatic affinity (olivine melilitites and olivine nephelinites, basanites, and possibly also carbonatites) which evolved independently to generate the observed spectrum of intrusive rocks of Sung Valley, located ~ 23 km north of NPJA. This observation seems to be applicable to the intrusions of picro-basalt, high Mg-tholeiite, tholeiite and alkaline dykes of NPJA with the exception of carbonatite; however minor carbonate ocelli occur in almost all samples. The cyclic evolution of picro-basalt into high Mg-tholeiitic basalt, tholeiitic basalt and basaltic andesite may have taken place through differentiated processes. While tephrite basanite; alkali olivine basalt and nephelinite with phenocrysts of olivine and diopside clearly demonstrate simultaneous evolution but, derived from a separate alkaline enriched mantle source comparable to Sung alkaline rocks also derived from an enriched mantle source through small scale partial melting caused by the Kerguelen Plume activity (Winter, 2001; Srivastava, 2004 & 2005; Melluso, et al, 2010). Alkaline OIB (Fig-13) are usually associated with: **i)** continental rift setting basalts caused by mantle plume activity; **ii)** the asthenosphere, **iii)** the lithospheric mantle and **iv)** the continental crust (Sun, & McDonough, 1989) which are keys to studying the petrogenesis. Relatively high Zr/Y ratios of the samples reflect higher incompatibility of Zr compared to Y in the mantle phases (Pearce & Norry, 1979; Nicholson & Latin (1992). Therefore, the NPJA dykes could have been generated by varying degrees of melting. The high Zr/Y (4.03- 11.4) ratios too, plausibly illustrate their derivation from: ***a)*** *an enriched mantle source* or, ***b)*** possible *contribution of a mantle plume* [OIB, Zr/Y = 9.66, E-MORB = 3.32; (Sun, & McDonough, 1989)] or, ***c)*** or, *derivation from a mantle metasomatized zone*: out of which the second option is more tenable due to involvement of the Kerguelen Plume (Ray & Pande, 2001; Srivastava, et al, 2004; Nambiar, 2007). Furthermore, the Zr/Nb ratio in volcanic rocks may reflect crustal contamination or, variation in degree of partial melting (Wilson, et al, 1995; Kamber & Collerson, 2000; Hagos, et al, 2010) which is only slightly elevated (4.32 to 12.83) in the NPJA samples, suggesting a relatively low degree of partial melting or, crustal involvement. Nb/La vs. La/Yb plot (Fig-15.1) however, inferred crustal involvement for the more evolved samples but overall most are generated through the lithospheric-asthenospheric mantle interaction (Fitton, et al, 1991 & Karsli, et al, 2014). At given Zr contents most of the samples have higher Nb, Th contents and Nb/Y ratio (Table-I & II); where Nb, considered to be more sensitive to variations in degrees of partial melting than Zr can be used to constrain the influence of variable degrees of melting (Kamber & Collerson, 2000). The Y/Nb ratio is another useful tool for determination of source generation, for which, some of the NPJA dykes may have been involved with a depleted mantle source while others are representative of more enriched source. The resulting picture is that the alkaline samples (tephrite basanite, alkali olivine basalt & nephelinite) possess the lowest Y/Nb values (Y/Nb = 0.42–0.72) among the investigated samples, while the wide variability in the tholeiitic dykes characterize relatively high to very high values of Y/Nb ratios (0.75 - 1.2) favouring contribution from enriched mantle sources in both cases. Furthermore, low Nb/La ratios (<1.0) in volcanic rocks are a reliable trace element index of crustal contamination (Kieffer, et al, 2006) corroborating to the low Nb/La ratio of NPJA dykes with the exception of the nephelinite with Nb/La=1.02 which is least contaminated. Similarly, La/Nb ratio can yet be another useful index of crustal contamination in magmas (Zhang, et al, 2002). However, contamination may also have been caused by mantle source heterogeneity (Zhang, et al, 2002). In general modest to high Nb values but strongly enriched Th of the samples infer crustal contamination through assimilation and fractional crystallization (AFC) [De Paolo, 1981] and/or, MASH (melting, assimilation, storage and homogenization) [Thompson, *et al*., 1984; Aldanmaz, et al, 2000]. Mild enrichment of incompatible elements and REE in B-2 and B-3 batches reflects only moderately differentiated and contaminated source as compared to B-1 samples which are less evolved. Compatible trace elements such as Ni and Cr (Fig-12) reveals positive correlation with Mg# reflecting the role of olivine in controlling their distribution as expected for fractionation and crystallization of mafic minerals *e.g.*, olivine, clinopyroxene and spinel. However, variability may be attributed to the varying phenocrysts matrix ratios rather than the composition of the parental magmas (Cox, 1980). Nevertheless, high Mg# usually means that magmas are yet to undergo fractional crystallization en route to the surface (De Paolo, 1981; Cox, 1980; Prestvik & Goles, 1985) and fractionation has a tendency to increase the incompatible element concentrations in basaltic magmas relative to those of the more MgO rich primary magmas (Zhang, et al, 2002). These observations are consistent with the high MgO, Mg#, Ni and Cr contents of the cumulitic to porphyritic textured picro-basalt, high Mg-tholeiite basalt and some tephrite basanite and alkali olivine basalt samples, probably derived from a primitive magmatic source (Table.-I & II) as compared to the more evolved tholeiitic basalt and basaltic andesite samples with lower MgO, Mg# and compatible element contents. The alkali olivine basalt are derived from a different deeper source through small scale partial melting of the and enriched mantle (Winter, 2001) which is evident from the Ba/Nb vs. La/Nb diagram [Fig-15] (Sun & McDonough, 1989; Kontak, et al, 2001). A negative Mg# vs. SiO_2, Mg# vs. Zr plots and positive Mg# vs. CaO plot (Fig-12), invoke normal magmatic differentiation while the Nb/Y vs. Zr/TiO_2 binary plot illustrates [Fig-14.1] a consistent alkali basalt origin (Winchester & Floyd, 1977).

Modest to abundant REE increases from picro-basalt, tholeiite to calc-alkaline samples invoking a stronger REE fractionation with increasing alkalinity. Absence of Eu anomalies suggested no involvement of

plagioclase in B-1 and B-2 while plagioclase fractionation characterized B-3. Similar REE profiles of primitive samples (picro-basalt and tephrite basanite) and evolved samples (tholeiitic basalt, basaltic andesite and alkali olivine basalt respectively) strongly suggest respective assimilation and fractional crystallization (AFC) and/or melting, assimilation, storage and homogenization (MASH) [De Paolo, 1981; Aldanmaz, et al, 2000] during the different episodic tholeiite and alkaline basaltic dyke activities in NPJA possibly corresponding to the different tholeiitic and alkali basalt volcanic effusion of Early Cretaceous Sylhet Trap (Talukdar, 1967 & 1971). Notable enrichment, in increasing order of REE from picritic to tholeiitic to alkaline dykes reflected the different dept of partial melting of these samples *or*, different rate of crystallisation and differentiation; with picro-basalt and alkaline samples tapped from a deeper mantle source for each batch. Higher REE contents in tephrite basanite, alkali olivine basalt denotes derivation from enriched mantle source corroborate by the Ba/Nb *vs.* La/Nb plot (Sun, & McDonough, 1989; Kontak, et al, 2001). While in basaltic andesite higher contents may have been caused by differentiation process. The nephelinite (NP) sample without Eu-anomaly affiliates with the B-2 batch. High Th/La ratio (0.5 to 1.2), a sensitive indicator of crustal interaction (Pearce, 1983; Taylor, & McLennan, 1985; Thompson, & Morrison, 1988; Sun, & McDonough, 1989) supports significant crustal contamination. The similarity of REE pattern of NPJA samples with those of Sylhet Trap Basalts of Mawsynram-Balat section (Ghatak & Basu, 2011) inferred to a common source [Fig-13.3]. High $(Gd/Yb)_{CN}$ ratios are indicative of garnet fractionation during formation (>60 km) because the HREE are partially coherent in the garnet phase (Hirschmann, & Stolper, 1996). The NPJA basalt dykes with $(Gd/Yb)_{CN} > 2$ could therefore be linked to mantle sources that melted at depths of the garnet facies suggesting presence of garnet as a residual phase in the source with only one picro-basalt sample exhibiting $(Gd/Yb)_{CN} < 2$ of spinel facies (Safonova, et al, 2011) [Fig-15.2 & 15.3]. This result is constant with considerable depleted HREE as compared to LREE $(La/Yb)_{CN}$. Interestingly, the $[Tb/Yb]_{CN}$ values of NPJA dykes vary between 1.29 and 2.38 corroborating to the alkaline basalts of Hawaii [$(Tb/Yb)_{CN}$ = 1.89–2.45] thought to be derived from a garnet bearing source due to hot spot activity (Sun & McDonough, 1989) as supported by the (Dy/Yb)N vs. (Ce/Yb)N diagram where samples clustered on the plume tie-line (Fig-15.2; Haase & Devey, 1996). High Dy/Yb ratios of 1.54 to 2.55 of the samples with respect to that of chondrite (Dy/Yb = 1.49; Sun, & McDonough, 1989) suggested a garnet-bearing lherzolite source for the derivation of these basalts as evidenced by the Tb/Yb vs. Ce/Yb plot (Fig-15.2) and (Dy/Yb)N vs. (Ce/Yb)N diagram (Fig-15.3). These observations correspond with the garnet peridotite sourced basalts of Mawsynram-Balat and Cherrapunjee-Shella sections of Khasi Hills (Ghatak & Basu, 2011), with the latter located ~ 25 km, WSW of NPJA (Fig-1) that were comparable to the Rajmahal-II type basalts (Ghatak & Basu, 2011).

The NPJA samples affiliates to an alkaline-OIB type (Fig-14 & 14.1) with Ba/Nb vs. La/Nb plot (Fig-15), signifying derivation from an EM type source (Sun & McDonough, 1989; Kontak, et al, 2001). Compatible trace elements such as Ni and Cr with high Mg# of picro-basalt, high Mg-tholeiitic basalt and the alkali olivine basalt samples favour a primitive magmatic source, while enriched Ba, Rb, Th and La of the more evolved samples invoke crustal involvement. The OIB nature of samples is expected, given that ensuing rifts commonly form above thermal anomalies or, mantle plumes, (Kontak, et al, 2001; White & McKenzie, 1989) are often accompanied by large amounts of magmatic activity (Ernst, et al, 1995) that in turn provide transport mechanism for ascent of OIB-type melts into continental regions (Kontak, et al, 2001). Mafic dykes, interpreted to have been formed from mixing of tholeiitic, OIB and alkaline high- to low-Ti alkaline magmas are reported from mid-Cretaceous (ca.107 Ma) dykes of northernmost Greenland associated with rifting of Antarctica and New Zealand (Kontak, et al, 2001) that in part resembles the NPJA network of dykes.

III. Discussions and Conclusions

The NPJA dykes intruding the Precambrians are of picritic to tholeiitic to alkaline and occasionally calc-alkaline in compositions. These are hypabyssal intrusives representative of the Early Cretaceous Sylhet Trap volcanism located ~ 25 km, WSW of the study area, caused by the Kerguelen Plume (Gupta & Sen, 1988; Storey, et al, 1992; Ray & Pande, 2001; Srivastava, et al, 2004; Nambiar, 2007). Intrusions took place during an extensional phase near to an intersection zone of the Raibah and Umngot Faults (Fig-1 & 2). Corroded xenocrystic grains and early formed macrocrysts of olivine and diopside indicate interaction between early formed materials with later melts (Fig-6 & 7). Cumulitic to highly porphyritic nature of picritic basalt (Fig-4) and alkali basalt and basanite dykes favours sudden and probably violent ascent from the mantle to the surface. Common occurrences of analcite ocelli with calcite inclusions in the alkali basalts (tephrite basanite, nephelinite), occasionally in tholeiitic basalts (tholeiitic basalt) and notable presence of calcite ocelli in other samples invoke immiscibility involving different sourced basic and alkaline magma with minor carbonate rich melts at some point of time during evolution of these dykes. A sulphide phase is associated with the more evolved andesitic basalt as evident by presence of pyrite ocelli inclusion within carbonate ocelli (Fig-10). Trace elements reveal both mantle and crustal signatures, consistent with AFC and MASH models [De Paolo, 1981; Aldanmaz, et al, 2000] while, REE studies inferred three pulses of dyke activities probably corresponding to the

different levels of basalt flows of Sylhet Traps with one high Mg-tholeiitic dyke showing a relative flat HREE enrichment and LREE depletion compared to other samples, indicative of its mantle origin. Collectively, the dykes have REE patterns compatible to the Mawsynram-Balat and Rajmahal-II basalts, both linked to the Kerguelen Plume activity (Takahahshi, et al, 1998; Ghatak & Basu, 2011, 2013) [Fig-16] as supported by the (Dy/Yb)N vs. (Ce/Yb)N diagram (Fig-15.2). Ba/Nb vs. La/Nb plot (Fig-15) suggested an EM type source; with $(Gd/Yb)_{CN}$ ratios > 2 linked to mantle sources that melted at depths of the garnet facies (>60 km); while the $[Tb/Yb]_{CN}$ ratios are in tune with the alkaline basalts of Hawaii also derived from a garnet bearing source due to hot spot activity (Fig-15, 15.2 & 15.3). These preliminary conclusions are however to be further confirmed with more futuristic detailed field work, petrography, geochemistry and more importantly isotope studies of these newly reported network/swarm of dykes and dykelets.

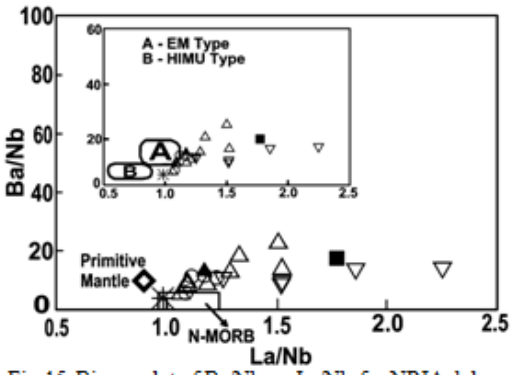

Fig-15: Binary plot of Ba/Nb *vs.* La/Nb for NPJA dyke-rocks compared to fields for HIMU and EM-type basalts (shown in the inset). Note a mild positive correlation among the samples. Symbols as in Fig-11.

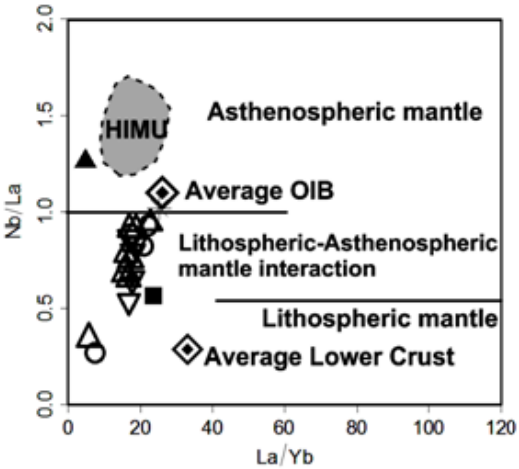

Fig-15.1: Nb/La vs. La/Yb variation diagram (Fitton, et al, 1991). Symbols as in Fig-11. Average OIB is taken from Fitton et al. (1991) and average lower crust is after Chen and Arculus (1995). Dashed lines separating fields of the asthenospheric, lithospheric and mixed mantle, and the HIMU-OIB field are after Smith et al. (1999) and Weaver et al. (1987), respectively.

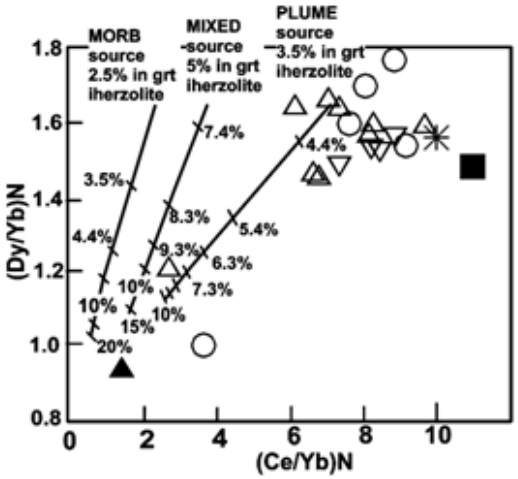

Fig-15.2: (Dy/Yb)N vs. (Ce/Yb)N diagram. Magma source lines and melting rate values after Haase & Devey (1996).

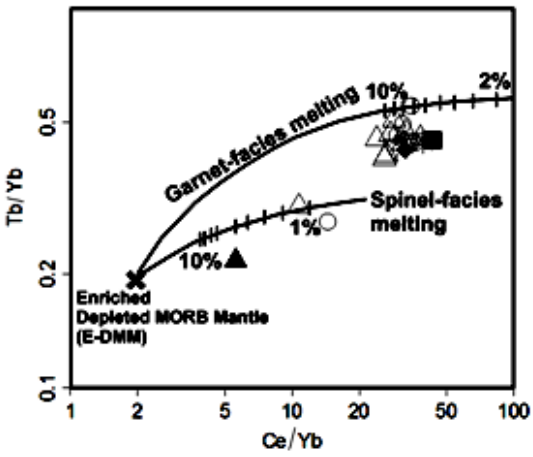

Fig-15.3: Partial melting models for the samples. Garnet- and spinel-facies melting curves after Walter, (1998) & Kinzler, (1997).

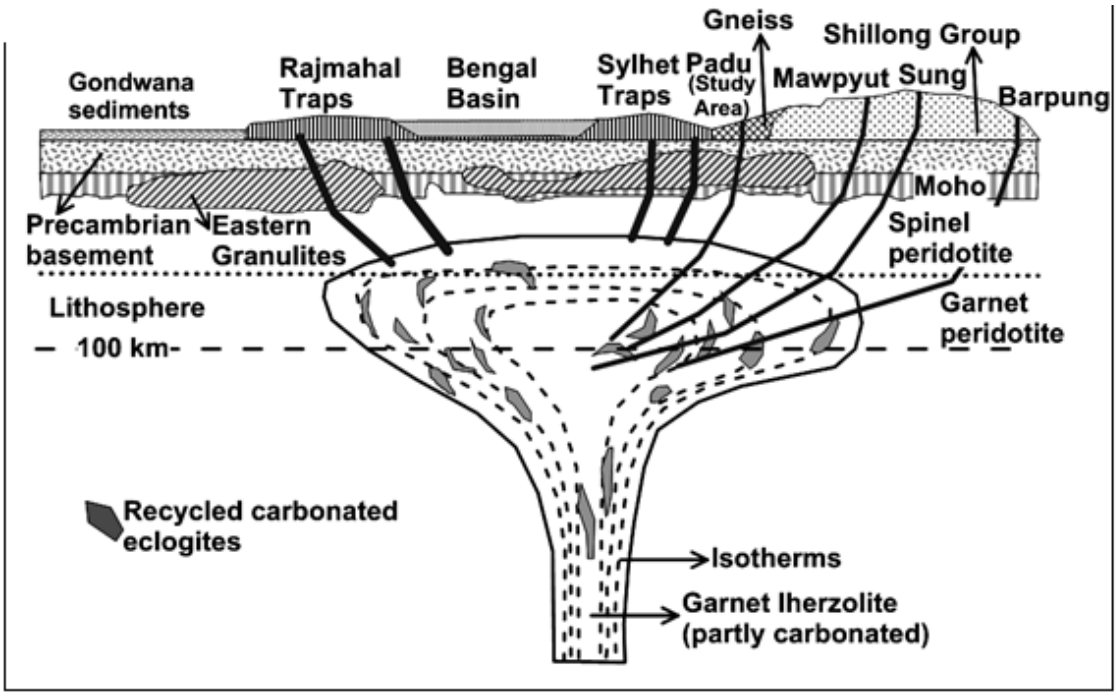

Fig-16. A model for the formation of the Rajmahal-Sylhet Flood Basalt Province. The mantle plume ascends with recycled eclogitized basalts now carbonated (Archaean) within it. The top of the plume head undergoes high degree of batch melting of the relatively primitive part of the plume in the stability field of spinel to form flood basalts. Lower degree melting of the carbonated relatively primitive peridotite at greater depths of gamet stability also occur to form some of the carbonatites and alkalic rocks including the alkaline dykes of the NPJA. Contamination of melts from carbonated eclogites are needed to account for the variable Nd, Sr, and Pb isotopes of the rest of the alkalic rocks with the lower degree melts in the Kerguelen plume. Diagram modified from Takahahshi et al. (1998) & Ghatak and Basu, (2013).

Acknowledgement

The authors express their gratitude to Shri. Amarjeet Singh, Addl. Director General, Shri. U. K. Behera, Addl. Director General (Retd), and Dr. Aparajita Datta, Superintendent Geologist, Geological Survey of India, North Eastern Region, for their continuous support and permission to publish the data. Fruitful consultations and discussions with Dr. Abhijit Roy, Superintendent Geologist, Eastern Region, Kolkata, are highly regarded and acknowledged. Deep appreciation goes to Shri. S. Tripathy, and Dr. S. Nandy, Geologists, GSI, CHQ, Kolkata for their valuable services during EPM Analysis. The support obtained from Officers and Staff-Members of Meghalaya Geology Projet and Petrology Division, GSI, NER, Shillong are highly regarded.

References

[1] **Aldanmaz, E., Pearce, J.A., Thirlwall, M.F., Mitchell, J.G. (2000):** Petrogenesis evolution of late Cenozoic, postcollision volcanism in western Anatolia, Turkey. *J. Volcanol. Geotherm. Res.*, 102: 67-95.

[2] **Chen, W., Arculus, R.J., (1995):** Geochemical and isotopic characteristics of lower crustal xenoliths, San Francisco Volcanic Field, Arizona, U.S.A. Lithos 110, 99–119.

[3] **Cox, K.G. (1980)**: A model for flood basalt volcanism. Jour. Pet. 21, 629-650.

[4] **Culler, R.L. & Graf, J.L. (1984):** Rare earth elements in igneous rocks of the continental crust: predominantly basic and ultrabasic rocks. In Rare Earth Element Geochemistry (P. Henderson, ed.). Elsevier, Amsterdam, Netherlands (237-274).

[5] **De Paolo, D.J. (1981):** Trace element and isotopic effects of combined wall-rock assimilation and fractional crystallization. *Earth Planet. Sci. Lett*., 53: 189-202.

[6] **Demeny, Attila; Harangi, Szabolcs; Forizs, Istvan and Nagy Geza (1997):** Primary and secondary features of analcimes formed in carbonate-zeolite ocelli of alkaline basalts (Mecsek Mts., Hungary): textures, chemical and oxygen isotope compositions. *Geochemical Journal*, Vol. 31 (No. 1), pp. 37-47.

[7] **Ernst, R.E., Head, J.W., Parfitt, E., Grosfils, E. & Wilson, L. (1995):** Giant radiating dyke swarms on Earth and Venus. *Earth Sci. Rev.* **39**, 1-58.

[8] **Fitton, J.G., James, D., Leeman,W.P. (1991):** Basic magmatism associated with Late Cenozoic extension in the western United States: compositional variations in space and time. Journal of Geophysical Research 96, 13693–13712.

[9] **Ghatak, A. & Basu A. R. (2011):** Vestiges of the Kerguelen plume in the Sylhet Traps, north-eastern, India, Earth Planet. Sci. Lett. (2011), 308, 52–64.

[10] **Ghatak, A. & Basu A. R. (2013):** Isotopic and trace element geochemistry of alkalic–mafic–ultramafic–carbonatitic complexes and flood basalts in NE India: Origin in a heterogeneous Kerguelen plume. Geochimica et Cosmochimica Acta 115, p. 46–72.

[11] **Gogoi, K. (1975)**: The geology of the Precambrian rocks in northwest part of the Khasi and Jaintia Hills, Meghalaya. Geol. Surv. Ind. Misc. Pub. No.23, pt. 1, pp: 37-48.

[12] **Green, D. H. (1969):** The origin of basaltic and nephelinitic magmas in the earth's mantle. *Tectonophysics, 7*, 409-22.

[13] **Gupta, R.P. and Sen, A.K. (1988):** Imprints of the Ninety East Ridge in the Shillong Plateau, Indian Shield, Tectonophysics, V-154 (1988) 335-341 Elsevier Sci. Pub. B.V., Amsterdam.

[14] **Haase, K.M., Devey, C.W., (1996):** Geochemistry of lavas from the Ahu and Tupa volcanic fields, Easter Hotspot, South Pacific: implications for intraplate magma genesis near a spreading axis. Earth Planet. Sci. Lett., **157**, 1–4, 129–143.

[15] **Hagos, M., Koeberl, C., Kabeto, K., & Koller F., (2010):** Geochemical characteristics of the alkaline basalts and the phonolite – trachyte plugs of the Axum area, northern Ethiopia, Austrian Jour. of Earth Sci. V - 103/2 pp-153-170.

[16] **Hirschmann, M.M. & Stolper, E.M. (1996):** A possible role for garnet pyroxenite in the origin of the "garnet signature" in MORB. Contrib. Mineral. Petrol. 124, 185–208.

[17] **Irvine,T.N., & Barager, W.R.A. (1971):** A guide to the chemical classification of the common volcanic rocks, Can. Jour. Earth. Sci. Vol. 8.

[18] **Kamber, B.S. & Collerson, K.D., (2000):** Zr/Nb systematics of ocean island basalts reassessed - The case for binary mixing. Journal of Petrology, 41, 1007–1021.

[19] **Kieffer, B., Arndt, N., Lapierre, H., Bastien, F., Bosch, D., Pecher, A., Yirgu, G., Ayalew, D., Weis, D., Jerram, A.D., Keller, F. & Meugniot, C., (2004):** Flood and shield basalts from Ethiopia: magmas from the African superswell. Jour. Petrology, 45, 793–834.

[20] **Kinzler, R.J. (1997):** Melting of mantle peridotite at pressures approaching the spinel to garnet transition: application to midocean ridge basalt petrogenesis. Journal of Geophysical Research 102, 853–874.

[21] **Khonglah, M.A., Khan, M.A., Karim, M.A., Kumar, A., & Choudhury, J. (2008)**: Geology and structure of the areas in and around Shillong, Meghalaya, North East India, revisited, Proceedings of the National Seminar on Geology & Energy Resources of NE India: Progress & Perspectives Nagaland University Res. Jour. Sp. Pub.

[22] **Khonglah, M.A. & Imtikumzuk (2010):** Specialized Thematic Mapping of Gabbroic Anorthosite and the associated Porphyritic Granite around Nongkasen- Nongstoin and also Myriaw-Synnia Area along with Parentage Studies of Gabbroic Anorthosite Rock, West Khasi Hills, Meghalaya. GSI, Rec. 143, pt-4, p. 14-20.

[23] **Khonglah, M.A., Anil Kumar, A., Mukherjee, P.K. & Haokip, L.T. (2012):** Specialized Thematic Mapping and Tectono Metamorphic Studies of the Gneiss-Quartzite/Schist Contact and their Stratigraphic Relation along the Eastern Margin of Shillong Basin in parts of East Khasi Hills and Jaintia Hills Districts, Meghalaya, Rec. GSI, V-145, pt-4.

[24] **Kontak, D. J., Jensen S.M., Dostal, J., Archibald, D.A., & Kyser T. K., (2001):** Cretaceous Mafic Dyke Swarm, Peary Land, Northernmost Greenland: Geochronology And Petrology, *The Canadian Mineralogist*, Vol. 39, pp. 997-1020.

[25] **Le Bas, M.L., Le Maitre, R.W., Streckeisen, A. & Zanettin, B., (1986):** A chemical classification of volcanic rocks based on the total alkali – silica diagram. Journal of Petrology, 27, 745 – 750.

[26] **Maitra, M., David, J.S., & Bhaduri, S. (2011):** Melanite garnet-bearing nepheline syenite minor intrusion in Mawpyut ultramafic-mafic complex, Jaintia Hills, Meghalaya. J. Earth Syst. Sci. 120, No. 6, pp. 1033-1041.

[27] **Mazumdar, S.K. (1976)**: A summary of the Precambrian Geology of the Khasi Hills, Meghalaya, GSI, Misc. Publication No. 23, pt- II, pp: 311-334.

[28] **Meschede, M. (1986):** A method of discriminating between different types of mid-ocean ridge basalt and continental tholeiites with the Nb-Zr-Y diagram. *Chem. Geol*., 56: 207-218.

[29] **Nakamura, N. (1974):** Determination of REE, Ba, Fe, Mg, Na and K in carbonaceous and ordinary chondrites. Geochim. Cosmochim. Acta. 38, 757-73.

[30] **Nambiar, A.R. (2007):** Early Cretaceous Lamprophyre dykes from Nongcharam Fault Zone, Meghalaya, Northeastern India, Geol. Soc. Ind. V-69, pp. 641- 652.

[31] **Nandy, D. R. (2001):** Geodynamics of North-Eastern India and the adjoining region. acb-publication, Culcutta.

[32] **Nicholson, H. & Latin, D. (1992):** Olivine tholeiites from Krafla, Iceland: evidence for variation in melt fraction within a plume. J. Petrol. 33:1105–1124.

[33] **Pearce & Norry, 1979:** Petrogenetic implications of Ti, Zr, Y and Nb variations in volcanic rocks. Contrib Mineral Petrol 69:33–47.

[34] **Pearce, J.A. (1983):** Role of the sub-continental lithosphere in magma genesis at active continental margins. In: Hawkesworth, C.J., Norry, M.J. (Eds.), Continental Basalts and Mantle Xenoliths, Shiva. Cheshire, UK, 230-249.

[35] **Prestvik, T. & Goles, G. G. (1985)**: Comments on the petrogenesis and the tectonic setting of Columbia River Basalts. Earth Planet. Sci. Lett. 72, 65–73.

[36] **Ray Jyotiranjan S., & Pande, Kanchan (2001):** ^{40}Ar-^{39}Ar age of carbonatite-alkaline magmatism in Sung Valley, Meghalaya, India. Proc. Indian Acad. Sci. (Earth. Planet. Sci.), 110, No. 3, pp. 185-190.

[37] **Safonova, I. Yu., Buslov, M.M., Simonov, V.A., Izokh, A.E., Komiya, T., Kurganskaya, E.V., & Ohno, T. (2011):** Geochemistry, petrogenesis and geodynamic origin of basalts from the Katun accretionary complex of Gorny Altai, *(southwestern Siberia)*, Elsevier, Russian Geology and Geophysics 52, 421-442.

[38] **Srivastava, K, Rajesh, & Sinha, A. K. (2004):** Early Cretaceous Sung Valley ultramafic-alkaline- carbonatite complex, Shillong Plateau, North-eastern India: petrological and genetic significance, Mineralogy and Petrology, Springer-Verlag, Austria 80: 241-263.

[39] **Srivastava Rajesh K., Heaman, Larry M., Sinha Anup K., Shihua Sun (2005):** Emplacement age and isotope geochemistry of Sung Valley alkaline–carbonatite complex, Shillong Plateau, northeastern India: Implications for primary carbonate melt and genesis of the associated silicate rocks. Lithos. 81, 33– 54.

[40] **Storey, M., Kent, R.W., Saunders, A.D., Hergt, J., Salters, V.J.M., Whitechurch, H., Sevigny, J.H., Thirlwall, M.F., Leat, P., Ghose, N.C., & Gifford, M. (1992):** Lower Cretaceous volcanic rocks on continental margins and their relationship to the Kerguelen Plateaus. In: Wise, S.W., Schlich, R. (Eds.), Proceedings of the Ocean Drilling Program. : Scientific Results, 120. Ocean Drilling Program, College Station, TX, pp. 33–53.

[41] **Sun, S.S., and McDonough, W.F. (Eds.), (1989):** Chemical and isotopic systematics of oceanic basalts: implications for mantle composition and processes. Geol. Soc. London Special Pub. U. K. 13-345 pp.

[42] **Sun, S.s. (1980):** Lead isotopic study of young volcanic rocks from mid-oceanic ridges, ocean islands and islands areas. Philosophical Transactions of the Royal Society of Londaon 297, 409-445.

[43] **Takahahshi E., Nakajima K. and Wright T. L. (1998)**: Origin of the Columbia River basalts: Melting model of a heterogeneous plume head. Earth Planet. Sci. Lett. 162, 63–80.

[44] **Talukdar, S.C. (1967):** Rhyolite and alkali basalt from the Sylhet trap Khasi Hills, Assam, Curr. Sci. No. 9, pp-238-239.

[45] **Talukdar, S.C. & Murthy, M.V.N. (1971):** The Sylhet traps, their tectonic history, and their bearing on problems of Indian flood basalt provinces, Bulletin Volcanologique, 1971, Volume 35, Issue 3, pp 602-618.

[46] **Taylor, S.R. & McLennan, S.M. (1985):** *The Continental Crust: Its Composition and Evolution*. Blackwell, Oxford, U.K.

[47] **Thompson, R.N., Morrison, M.A., Hendry, G.L., Parry, S.J. (1984):** An assessment of the relative roles of crust and mantle in magma genesis: an element approach. Philos. Trans. Royal Soc. London Ser. A, 310: 549-590.
[48] **Thompson, R.N. & Morrison, M.A. (1988):** Asthenospheric and lower-lithospheric mantle contributions to continental extensional magmatism: an example from the British Tertiary Province. *Chem. Geol.* 68, 1-15.
[49] **Walter, M.J., (1998)**: Melting of garnet peridotite and the origin of komatiite and depleted lithosphere. Journal of Petrology 39, 29–60.
[50] **White, W.M., McKenzie, D.P. (1989):** Magmatism at rift zones: the generation of volcanic continental margins and flood basalts. J. Geophys. Res., 94: 7685-7729.
[51] **Wilson, M., Downes, H. and Cebriá, J., (1995):** Contrasting fractionation trends in coexisting continental alkaline magma series; Cantal, Massif Central, France. Journal of Petrology, 36, 1729 –1753.
[52] **Winchester, J., & Floyd, P.A. (1977):** Geochemical discrimination of different magma series and their differentiation products using immobile elements. *Chem. Geol*., 20: 325- 343.
[53] **Zhang Zhaochong, Feng Chengyou, Li Zhaonai, Li Shucai, Xin Ying, Li Zhaomu & Wang Xianzheng (2002):** Petrochemical study of the Jingpohu Holocene alkali basaltic rocks, northeastern China, Geochemical Journal, Vol. 36, pp. 133 to 153.

Table-I: Whole rock analyses of B1 basaltic dykes

Sl No.	B1/1	B1/2	B1/3	B1/4	B1/5	B1/6	B1/7	B1/8	B1/9	B1/10
Sample	AJ-6A (m)	UMT-1B	ML-2	NH-3A	PN-1D (L)	UMT-3A	NH-1F	AJ-1G	UMT-3B	ML-2A
Field description	Cumulitic to Porp. Basalt	Porp. Basalt	Porp. Basalt	Porp. Basalt	Porp. Basalt	Porp. Basalt	Porp. Basalt	Porp. Basalt	Porp. Basalt	Porp. Basalt
Le Bas, (1980)	TB	TB	TB	TB	TB	TRB	TB	TBN	AB	AB
De la Roche, (1980)	TB	PB	PB	BS	BS	BSN	AB	PB	AB	PB
Jensen, (1976)	KM	KM	KM	KMBS	KMBS	HMTB	KM	KM	KM BS	HMTB
SiO_2%	46.92	42.98	41.14	41	47.97	46.56	44.45	41.26	42.82	43.16
Al_2O_3 %	5.55	4.55	5.26	11	14.08	13.02	11.14	11.5	9	11.2
Fe_2O_3 (T)%	8.44	9.57	11.89	12.23	9.42	9.32	10.72	12.23	10.26	10.14
NPO %	0.13	0.14	0.14	0.15	0.18	0.32	0.14	0.15	0.17	0.15
MgO %	16.13	19.81	19.13	11.91	9.34	6.72	9.08	9.31	10.6	11.29
CaO %	10.31	11.11	10.02	9.55	9.14	10.04	10.47	12.49	11.57	11.64
Na_2O %	0.78	0.91	0.55	1.47	2.64	2.3	3.41	1.99	2.04	2.06
K_2O %	0.45	0.5	0.39	1.31	1.2	1.46	1.86	1.14	1.63	1.34
TiO_2 %	1.4	0.86	0.97	1.4	0.96	1.56	1.56	1.77	1.46	1.54
P_2O_5 %	0.23	0.2	0.19	0.38	0.34	0.39	0.48	0.5	0.36	0.49
L.O.I. %	7.22	7.11	7.39	5.91	2.07	6.12	4.3	4.76	6.98	4.33
Na_2O/K_2O	1.73	1.82	1.41	1.12	2.20	1.58	1.83	1.75	1.25	1.54
Mg#	67.98	69.70	64.13	51.97	52.42	44.48	48.48	45.82	53.44	55.30
Norm										
Q	3.87	0	0	0	0	3.02	0	0	0	0
Or	2.95	3.26	2.57	8.57	7.45	9.42	11.79	7.3	10.72	8.52
Ab	7.3	8.49	5.18	13.74	23.42	21.2	16.31	11.54	13.67	13.92
An	11.4	7.55	11.95	21.59	24.13	22.75	10.26	20.63	11.75	18.63
Ne	0	0	0	0	0	0	7.9	3.62	2.98	2.6
Di wo	18.26	21.7	17.64	11.85	8.93	12.15	17.7	18.08	20.77	16.86
Di en	15.74	18.71	15.21	10.21	7.7	10.47	15.26	15.59	17.91	14.53
Hy en	28.9	9.97	19.35	6.58	15.8	7.85	0	0	0	0
Ol fo	0	18.18	13.14	11.3	0.71	0	6.35	6.73	8.1	11.07
Mt	0.47	0.5	0.51	0.54	0.62	1.14	0.49	0.53	0.62	0.53
He	9.02	10.21	12.91	13.15	9.46	9.38	11.15	12.88	10.99	10.54
Ap	0.56	0.48	0.46	0.92	0.78	0.93	1.12	1.18	0.87	1.15
Totals	98.45	99.05	98.92	98.45	98.99	98.3	98.33	98.09	98.38	98.35

PB - picrite basalt, TB - tholeiitic basalt, AB - alkali olivine basalt, TBN - tephrite basanite, TRB-trachy-basalts, KM – Komatiite, KMBS - komatiitic basalt & HMTB – high magnesian tholeiite basalt, AB – andesi-basalt. Comparative classification by De Roche, et al, (1980) and Jensen, (1976), provided in 4th & 5th row respectively. **Sample locations**: B/1 – Umsiang R. (Padu), B/2 & 8 – north of Ummatong, B/3, 7 & 9 – NNW of Mawlong; B/4 & 5 - Nongryngkoh

Table-II: Whole rock analyses of porphyritic basaltic dykes, tephrite basanite and basalt dykes of B2 and B3.

Sl No.	B2/1	B2/2	B2/3	B2/4	B2/5	B2/6	B3/1	B3/2	B3/3	B3/4	B3/5	B3/6
Sample	**NH-3E**	**UMT-4B**	**NH-4A(L)**	**UMT-3**	**NH-3C**	**UT-5**	**Mb-2**	**ML-2A [i]**	**AJ-1D1**	**ML-3A(L)**	**ML-3A(B)**	**SJ-3**
Field description	Porp. Basaltic dyke	Porp. Basaltic dyke	Porp. Basaltic dyke	Porp. Basaltic dyke	Basic dyke	Non-Porp. Basalt	Porp. Basaltic dyke	Porp. Basaltic dyke	Porp. Basaltic dyke	Porp. Basaltic dyke	Non-Porp. Basalt	Andesitic basalt
Le Bas	TB	TB	AB	AB	TBN	BA	APB	TBN	TBN	AB	TB	BA
De la Roche	TB	AB	PB	BS	NP	A	PB	AB	PB	BS	BS	LB
Jensen (1986)	KM BS	KM BS	KM BS	HMTB	HMTB	BS	KM	KM BS	KM BS	KM BS	KM BS	HFTB
SiO_2%	44.52	44.92	42.71	42.43	40.66	51.5	40.81	41.32	41.18	44.55	49.21	44.01
Al_2O_3 %	7.42	8.97	9.16	12.84	12.35	14.74	7.39	10.51	9.33	11	14.72	11.67
Fe_2O_3 (T)%	11.41	12.53	10.28	11.16	11.12	10.33	10.67	12.17	10.84	10.42	9.66	9.53
NPO %	0.24	0.16	0.13	0.14	0.17	0.18	0.13	0.16	0.14	0.14	0.14	0.16
MgO %	15.36	11.64	8.93	8.77	8.4	4.61	19.64	12.8	13.44	9.28	5.57	3.57
CaO %	8.52	7.68	13.99	10.05	11.82	6.86	10.19	11.3	11.55	10.58	10.05	7.24
Na_2O %	1.25	0.95	2.11	2.34	4.26	2.31	0.82	1.87	1.43	2.93	2.7	1.07
K_2O %	0.78	0.95	0.81	1.81	2.09	1.89	1.51	1.2	2.3	1.35	1.6	2.55
TiO_2 %	1.85	2.35	1.5	1.68	1.57	2.11	1.95	1.46	2.35	1.65	1.74	2.76
P_2O_5 %	0.3	0.37	0.33	0.53	0.69	0.32	0.17	0.45	0.37	0.33	0.3	0.44
L.O.I. %	6.24	6.5	7.76	5.42	4.34	3.44	5.32	5.18	5.11	6.09	2.28	14.11
Na_2O/K_2O	1.60	1.00	2.60	1.29	2.04	1.22	0.54	1.56	0.62	2.17	1.69	0.42
Mg#	59.93	50.79	49.11	46.61	45.63	33.15	67.16	53.89	57.94	49.74	39.05	29.39
Norm												
Q	0	7.51	0	0	0	12.4	0	0	0	0	3.8	13.58
Or	5.03	6.21	5.33	11.67	10.9	11.79	9.57	7.65	14.64	8.66	9.89	18.17
Ab	11.53	8.87	13.48	17.09	0	20.58	3.19	8.33	0.81	21.27	23.85	10.9
An	13.43	19.2	14.57	20.87	9	25.54	12.86	18.01	13.14	13.93	24.33	23.45
Lc	0	0	0	0	1.86	0	0	0	0	0	0	0
Ne	0	0	3.44	2.42	20.95	0	2.3	4.72	6.61	3.02	0	0
Di wo	12.85	8.56	25.24	12.56	20.72	3.5	16.81	17.71	19.28	17.07	10.84	6.98
Di en	11.08	7.38	21.76	10.83	17.86	3.01	14.5	15.27	16.62	14.72	9.34	6.02
Hy en	30.2	24.77	0	0	0	9.14	0	0	0	0	5.21	4.73
Ol fo	0.43	0	2.14	9.15	3.28	0	26.7	13.45	13.67	7.31	0	0
Mt	0.86	0.58	0.47	0.5	0.6	0.62	0.46	0.56	0.49	0.5	0.48	0.63
He	11.86	13.44	11.1	11.82	11.53	10.46	11.12	12.73	11.33	10.96	9.77	11.05
Ap	0.71	0.89	0.8	1.26	1.62	0.74	0.4	0	0.87	0.78	0.68	1.16
Totals	97.99	97.41	98.33	98.17	98.32	97.78	97.91	98.43	97.47	98.21	98.18	96.68

APB – alkaline picro-basalt, TB - tholeiitic basalt, PB- picro-basalt, AB - alkali basalt, TBN - tephrite basanite, TRB-trachy-basalts, BA - basaltic andesite, NP-nephelinite, KM - komatiite, KMBS - komatiitic basalt, HMTB - high magnesian tholeiite basalt, HFTB - high Fe tholeiite basalt, BS – basalt, AB - andesi-basalt, LB - Lati-basalt, A - andesite. Comparative classification by De la Roche, et al, (1980) & Jensen, (1976), provided in 4th & 5th row respectively. **Sample locations**: B2/2, B2/5, & B2/ 6 - north of Ummatong; B3/1 to B3/5 – North of Mawlong; B2/1, B2/3 & B2/4 – Nongryngkoh; B3/6 – Umngot R. west of Jarain

Table-III: Trace and REE in basaltic dyke rocks of NPJA

Sl No.	B1/1	B1/2	B1/3	B1/4	B1/5	B1/6	B1/7	B1/8	B1/9	B1/10	B2/1	B2/2	B2/3	B2/4	B2/5	B2/6	B3/1	B3/2	B3/3	B3/4	B3/5	B3/6
Ba	253	183	256	381	521	416	636	413	534	339	345	428	376	416	441	727	217	339	337	333	366	843
Ga	25	17	24	23	26	30	26	24	23	23	25	25	24	30	23	31	24	23	17	25	28	24
Sc	41	38	38	38	46	33	38	37	44	23	41	42	36	33	30	23	21	23	38	31	30	18
V	356	275	308	362	294	370	394	484	430	404	437	443	441	370	493	328	294	404	421	457	482	499
Th	15	11	15	20	15	10	21	19	19	15	22	12	15	10	20	18	17	15	12	14	15	8
Pb	2	2	4	5	4	10	2	7	2	2	4	2	8	10	13	20	2	<2	0	2	2	5
Ni	674	681	950	494	157	160	197	173	266	480	743	520	264	160	92	64	875	480	449	233	185	27
Co	81	91	100	73	64	65	62	69	56	71	79	77	69	65	61	26	95	71	64	62	58	35
Rb	3	34	32	47	12	77	42	43	79	54	31	21	38	77	50	121	32	54	33	47	69	212
Sr	290	301	393	555	446	803	672	859	616	570	444	361	628	803	1165	628	348	570	474	687	702	335
Y	16	11	18	24	30	27	27	22	24	20	19	23	20	27	25	38	16	20	18	25	25	32
Zr	141	86	109	164	121	247	238	225	176	164	169	233	175	247	259	372	90	164	148	193	227	366
Nb	16	15	15	24	5	46	25	36	25	28	24	31	26	46	60	29	13	28	25	28	29	42
Cr	1453	1122	1344	743	74	272	304	150	455	591	975	937	449	272	64	33	1323	591	791	332	231	25
Cu	46	67	80	130	18	166	125	180	170	172	113	68	171	166	150	31	72	172	132	169	166	15
Zn	94	79	101	95	155	115	118	106	96	96	107	118	116	115	139	146	73	96	102	115	125	111
Zr/Y	8.81	7.82	6.06	6.83	4.03	9.15	8.81	10.23	7.33	8.20	8.89	10.13	8.75	9.15	10.36	9.79	5.63	8.20	8.22	7.72	9.08	11.44
Zr/Nb	8.81	5.73	7.27	6.83	24.20	5.37	9.52	6.25	7.04	5.86	7.04	7.52	6.73	5.37	4.32	12.83	6.92	5.86	5.92	6.89	7.83	8.71
Y/Nb	1.00	0.73	1.20	1.00	6.00	0.59	1.08	0.61	0.96	0.71	0.79	0.74	0.77	0.59	0.42	1.31	1.23	0.71	0.72	0.89	0.86	0.76
Nb/Y	1.00	1.36	0.83	1.00	0.17	1.70	0.93	1.64	1.04	1.40	1.26	1.35	1.30	1.70	2.40	0.76	0.81	1.40	1.39	1.12	1.16	1.31
Y/Nb	1.00	0.73	1.20	1.00	6.00	0.59	1.08	0.61	0.96	0.71	0.79	0.74	0.77	0.59	0.42	1.31	1.23	0.71	0.72	0.89	0.86	0.76
Nb/Th	1.07	1.36	1.00	1.20	0.33	4.60	1.19	1.89	1.32	1.87	1.09	2.58	1.73	4.60	3.00	1.61	0.76	1.87	2.08	2.00	1.93	5.25
Ba/Th	16.87	16.64	17.07	19.05	34.73	41.60	30.29	21.74	28.11	22.60	15.68	35.67	25.07	41.60	22.05	40.39	12.76	22.60	28.08	23.79	24.40	105.38
REE																						
La	18.71	16.39	22.81	30.82	14.54	48.64	37.54	39.22	33.16	33.15	26.72	37.86	30.38	49.75	58.78	-	24.05	33.66	31.16	42.36	44.07	74.35
Ce	35.68	28.42	32.94	51.22	28.02	81.41	65.26	67.84	52.11	56.37	48.69	61.87	51.56	80.78	91.39	-	41.3	62.67	57.54	77.45	80.6	136.57
Pr	5.57	3.87	5.23	6.94	4.16	10.53	8.85	9.01	7.46	7.48	6.79	10.03	6.99	10.88	11.59	-	5.58	7.84	7.22	10.01	10.2	17.75
Nd	23.61	15.45	20.38	27.12	17.88	39.21	34.17	34.69	29.28	29.07	27.03	40.70	27.30	40.08	42.34	-	19.24	26.93	24.93	33.89	35.26	59.48
Eu	1.55	1.01	1.34	1.67	1.61	2.25	2.07	2.13	1.82	1.87	1.78	2.45	1.92	2.23	2.48	-	0.91	1.22	1.16	1.34	1.75	2.39
Sm	6.12	5.38	6.42	7.51	7.30	11.87	9.16	8.87	13.25	8.31	6.66	8.72	6.70	8.14	9.52	-	4.09	5.62	5.31	7.09	7.5	12.67
Gd	4.25	2.94	3.84	5.28	4.37	6.87	6.49	6.21	5.53	5.26	5.03	6.82	5.22	6.74	7.40	-	4.34	5.95	5.68	7.59	7.63	11.27
Tb	0.68	<0.50	0.62	0.80	0.79	0.98	1.01	0.94	0.88	0.82	0.76	0.99	0.80	0.99	1.04	-	0.62	0.81	0.77	1.04	1.06	1.43
Dy	3.80	2.50	3.48	4.34	4.90	5.30	5.68	5.16	4.85	4.32	4.06	4.88	4.27	5.32	5.64	-	3.31	4.36	4.1	5.61	5.7	7.3
Ho	0.71	<0.50	0.61	0.79	0.94	0.92	1.02	0.91	0.86	0.76	0.70	0.86	0.76	0.96	0.99	-	0.6	0.78	0.74	1	1	1.29
Er	2.09	1.12	1.58	2.09	2.70	2.45	2.75	2.39	2.19	1.99	1.79	2.16	1.99	2.49	2.68	-	1.57	2.11	1.93	2.7	2.66	3.5
Tm	<0.50	<0.50	<0.50	<0.50	<0.50	<0.50	<0.50	<0.50	<0.50	<0.50	<0.50	<0.50	<0.50	<0.50	<0.50	-	<0.5	<0.5	<0.5	<0.5	<0.5	0.53
Yb	2.47	0.98	1.36	1.92	2.62	2.14	2.50	2.12	1.88	1.74	1.54	1.78	1.73	2.24	2.33	-	1.43	1.8	1.73	2.38	2.49	3.17
Lu	<0.50	<0.50	<0.50	<0.50	<0.50	<0.50	<0.50	<0.50	<0.50	<0.50	<0.50	<0.50	<0.50	<0.50	<0.50	-	<0.5	<0.5	<0.5	<0.5	<0.5	0.5
Nb/La	0.86	0.92	0.66	0.78	0.34	0.95	0.67	0.92	0.75	0.84	0.90	0.82	0.86	0.92	1.02	-	0.54	0.83	0.80	0.66	0.66	0.56
Dy/Yb	1.54	2.55	2.55	2.26	1.87	2.48	2.27	2.43	2.58	2.49	2.64	2.74	2.47	2.38	2.42	-	2.31	2.42	2.37	2.36	2.29	2.30
$(La/Yb)_N$	5.06	11.11	11.16	10.69	3.70	15.15	9.99	12.33	11.78	12.73	11.57	14.19	11.73	14.83	16.80	-	11.21	12.47	12.01	11.87	11.80	15.64
$(Gd/Yb)_N$	1.37	2.38	2.25	2.19	1.33	2.56	2.07	2.34	2.35	2.42	2.61	3.05	2.41	2.40	2.53	-	2.53	2.63	2.62	2.54	2.44	2.83
$(Tb/Yb)_N$	1.29	2.38	2.13	1.94	1.41	2.14	1.88	2.07	2.19	2.21	2.32	2.60	2.16	2.08	2.09	-	2.03	2.11	2.08	2.05	1.99	2.11
$(Dy/Yb)_N$	0.99	1.63	1.64	1.45	1.20	1.59	1.45	1.56	1.66	1.60	1.69	1.76	1.59	1.53	1.55	-	1.48	1.55	1.52	1.51	1.47	1.48
Th/La	0.80	0.67	0.66	0.65	1.03	0.21	0.56	0.48	0.57	0.45	0.82	0.32	0.49	0.20	0.34	-	0.71	0.45	0.39	0.33	0.34	0.11

Sample nos. same as in Table-I & II